Biofouling in reverse osmosis processes: the roles of flux, crossflow velocity and concentration polarization in biofilm development

Suwarno, S. R.[a,c,1], Chen, X.[b,d,1], Chong. T. H.[a], McDougald, D. [b,d,e], Cohen, Y.[d,f], Rice, S. A. [d,e,f], Fane, A. G.[a,c,*]

a Singapore Membrane Technology Centre, Nanyang Environment and Water Research Institute, Nanyang Technological University, Singapore 637141, Singapore

b Advanced Environmental Biotechnology Centre, Nanyang Environment and Water Research Institute, Nanyang Technological University, Singapore 637141, Singapore

c School of Civil and Environmental Engineering, Nanyang Technological University, Singapore 639798, Singapore

d School of Biological Sciences, Nanyang Technological University, Singapore 637551, Singapore

e The Centre for Marine Bio-Innovation, The School of Biotechnology and Biomolecular Sciences, The University of New South Wales, Sydney NSW Australia 2052

f The Singapore Centre for Environmental Life Sciences Engineering, Nanyang Technological University, Singapore 637551, Singapore

[1] These authors contributed equally to this work

* Corresponding author (agfane@ntu.edu.sg Tel: 65-67905272 Fax: 65-67910676)

Abstract

Biofilm development in a spacer-filled reverse osmosis membrane channel can influence both trans-membrane pressure (TMP) and channel pressure drop ($\Delta P_{CH)}$. While current pretreatment methods are unable to completely tackle the biofouling problem, more insights are required to provide strategies to minimize the problem. This study examined the role of operating parameters (i.e. flux and crossflow velocity) to minimize biofouling in RO processes. The experiments were conducted with a lab-scale high pressure flat sheet RO reactor where changes in pressure drop along the channel and across the membrane were measured. The impact of biofouling was measured at constant fluxes, where the TMP rise and ΔP_{CH} rise and the biofoulant was quantified as biovolumes of live and dead bacteria on autopsied membrane and spacer samples by confocal laser scanning microscopy (CLSM).

The results show that TMP rise increased exponentially with increasing flux, and decreased with increasing crossflow velocity. The channel pressure drop, ΔP_{CH}, increased when either flux or crossflow velocity were increased, and was more dependent on crossflow. The biofoulant volume on the membrane increased with flux and was less dependent on crossflow. The biofoulant associated with the spacer was much less than on the membrane and relatively insensitive to flux or crossflow velocity.

The TMP rise could be correlated with the estimated concentration of nutrient at the membrane surface, $C_{w,N}$, highlighting the combined roles of flux and crossflow velocity in solute concentration polarization. Previous TMP rise data could also be correlated to the estimated $C_{w,N}$ values. This observation suggests a biofouling mitigation strategy by controlling both incoming nutrient concentration and operating conditions (flux and crossflow).

Keywords: Reverse osmosis, biofouling, biofilm, spacers, concentration polarization

1. Introduction

With the world facing water shortages, desalination technology with reverse osmosis (RO) is getting more attention. In the RO process, biofouling remains as one of the most difficult challenges to this technology. One feature of biofouling is the presence of a biofilm on the membrane that increases resistance and reduces membrane performance (water permeation and rejection of solutes). Biofilms consist of bacteria within extracellular polymeric substances (EPS) which help to provide structure for the biofilm and also play an important role in protecting bacteria from environmental stresses [1].

The development of biofilms in RO modules is affected by three sets of factors. The first factor is the biofouling potential in the feed water, which mainly includes the nutritional load and to a lesser degree the bacterial load [2]. The second set of factors are the operating conditions used in the RO, which include flux and crossflow velocity [3-5]. The third set of factors are membrane properties, such as surface charge, contact angle and rugosity, that may influence initial surface conditioning. This paper considers the first two factors.

A traditional and popular method to control biofouling is disinfection by chemicals (e.g. chloramine) and media filtration. Several other advanced methods (e.g. ozone and ultraviolet, UV) have been recently proposed as biofouling control strategies due to their ability to minimize wide-range of microorganisms and produce minimum byproducts. Although some successes have been reported, the biofouling problem in RO processes remains [6-8].

A recent review by Gutman et al. suggested that biofilms in the RO channel affect membrane performance both vertically (flux – membrane related) and horizontally (channel pressure drop – spacer related) [9]. A biofilm on the membrane surface (i.e. membrane biofouling) can cause an increase in trans-membrane pressure (TMP) due to hydraulic resistance and biofilm enhanced osmotic pressure (BEOP) [4, 10]. Flux plays an important role in membrane biofouling as it can affect the initial attachment of bacteria and also directly influences the surface concentration of solutes (including nutrients), as a result of concentration polarization (CP). Herzberg and Elimelech show in their study that the number of live bacteria cells are dominating over dead cells near the membrane surface which probably caused by the increased nutrient

concentration due to CP [11]. Crossflow velocity also plays an important role in membrane performance as it affects the shear stress on the membrane surface and influences CP through the boundary layer mass transfer. In our group's previous studies without spacer [3], and with spacer [12], membrane biofouling was observed to be more pronounced at higher flux and lower crossflow velocity. It was shown that fouling, measured as TMP rise, was less pronounced in the presence of a flow channel spacer, and that channel pressure deltaP, ΔP_{CH}, rise was relatively small. The paper [12] also speculated on the role of flux and crossflow in dTMP/dT and d ΔP_{CH}/dT, and in the case of ΔP_{CH} we suggested an increase with crossflow and no effect due to flux. The previous study used relatively high fluxes (20 – 40 L/m^{2}h) [12], and we now consider a lower range, more typical of desalination operating conditions (< 20 L/m^{2}h) [13], to test the assumed responses of TMP and ΔP_{CH}. The role of nutrient concentration polarization in TMP rise is also examined. Biofoulant volumes from CLSM observation provide supportive information which shows that biofilm accumulation on the membrane surface, and not on the spacer filaments, can be correlated to TMP and ΔP_{CH} increases. Additionally, it is shown that the flux dynamics may influence the ΔP_{CH} of the RO system.

2. Materials and methods

2.1. Reverse osmosis biofouling set-up

Two identical stainless steel RO cells were arranged in series, where each plate was 310 x 60 x 0.8 mm with an effective area of 0.0186 m^2 (described in [12]). The feed solution was delivered using a high pressure pump (CAT PUMP, model 227). System pressure and flow rate were controlled by a back pressure regulator (Swagelok, model KBP) and a flow control valve (Cole Palmer, model CP-32505-40), respectively. The pressures of feed and permeate streams were monitored by pressure transducers (Bourdon Haenni, model E913). Differential pressure transmitters (Yokogawa, model JX110A), with a ± 0.12% error, were used to monitor the channel pressure drop. The distance between the two differential pressure transmitter ports was 20 cm. Based on several repeat experiments the measured TMP and ΔP_{CH} values were ± 15%. A mass-flow controller (Brooks Instrument, model 5882) was installed on the permeate side to maintain constant flux during experiments.

Pseudomonas aeruginosa PAO1, from a stock solution grown in Nutrient Broth (NB) (Difco NB – BD Diagnostics), was introduced into the system using an injection

pump (ELDEX, model 5979-OptosPump 2HM) to deliver a final concentration of ~10^5 CFU/mL. The bacterial stock solution was prepared based on the method as described elsewhere [12]. The feed solution was fully recycled, and microfilters (KAREI, 5 and 0.2 μm for concentrate and 0.2 μm for bypass) were installed on the return bypass and retentate flows to prevent excess bacteria from entering the feed tank.

2.2. Biofouling experimental protocols

Before each experiment, RO flat sheet membranes (DOW Filmtec. BW-30), membrane support layers, and feed spacers (Hydraunautics, LFC-1) were soaked in ultrapure water (Merck-Millipore, Milli-Q) for 12 h and subsequently in 70% ethanol solution (Merck) for 1.5 h. To ensure stable condition for the biofouling experiments, prepared membranes were compacted at 65 L/m^2/h overnight with Milli-Q water. Following compaction, the water was replaced with fresh Milli-Q and the flux was set to the desired value. Subsequently, NaCl (Merck) was added to achieve a background salt concentration of 4000 mg/L and the system was allowed to mix for 1.5 h. NB solution was then added to provide a background nutrient concentration of 20 mg/L (equivalent to 6.5 mg/L total organic carbon, TOC) and the system was again allowed to mix for 1.5 h. TOC analyzer (Shimadzu, TOC-V) was used for the measurement of TOC.

Experiments were initiated by continuous injection of the *P. aeruginosa* stock solution. The biofilm was allowed to develop in the RO cell for 10 d, and both TMP and ΔP_{CH} were continuously measured using a data logging system. The feed solution was replenished twice daily with freshly medium. Upon completion of each experiment, membrane and spacer samples were taken for autopsy.

2.3. Membrane and spacer autopsies

The autopsied membrane and spacer samples were observed by confocal laser scanning microscope (CLSM). The samples were obtained from the same location in all of the experiments (10 cm from outlet). Biofilms were prepared for CLSM by staining with the LIVE/DEAD BacLight Bacterial Viability Kit (Molecular Probes, L7012) in accordance with the manufacturer's specifications. Microscopic observation and image acquisition of biofilms were performed using a CLSM (ZEISS, model LSM710), equipped with Argon laser at 488 nm and DPSS561-10 laser at 561 nm. Images were captured using the confocal microscope bundled program ZEN 2009

independently for both laser rays to provide comparison of live and dead cells in the biofilms. Thirteen images were taken per sample and stitched together with Office Visio (version 2007, Microsoft Corporation). The biovolumes ($\mu m^3/\mu m^2$) were calculated using IMARIS (version 7.1.1, Bitplane, Switzerland). Based on two repeat experiments of two selected conditions, the measured biovolumes error was ± 30%.

3. Results and discussion

3.1. Impacts of hydrodynamic conditions on pressure drop increases in RO

Reports have shown that in the event of biofouling, increases of pressure drops across the membrane (TMP) and along the feed channel (ΔP_{CH}) are experienced [14, 15]. For a system operating at constant feed flow rate and constant production rate (constant average flux), increase of both pressure drops signifies higher requirement of pump delivery pressure to maintain the permeate production [12].

3.1.1. Impact of flux

Three separate experiments were conducted at fluxes of 5, 10, and 15 L/m^2h (LMH) while superficial crossflow velocity was fixed at 0.17 m/s. Figure 1a shows the normalized TMP/TMP_0 profiles of the tests performed. The increase of TMP was relatively linear and the rate increased with flux. After 10 d, the TMP increase was 5%, 7%, and 13% for fluxes of 5, 10, and 15 LMH, respectively. The incremental TMP rise ($TMP-TMP_0$) plotted in Figure 1b shows the contribution of different fluxes to the amount of pressure required to maintain constant flux. After 10 d, the TMP rose by 0.3, 0.5, and 1.1 bar at fluxes of 5, 10, and 15 LMH, respectively.

Operation at higher flux is subject to a more severe biofouling. The flux induces convective transport of bacteria, nutrients, and solutes to the membrane surface resulting in faster biofilm development on the membrane [3]. The data in Figure 1b may be further processed to produce the TMP rise rate by calculating the ratio of the total TMP rise (bar) and the total time needed (day). Figure 2 shows the increased rate of TMP rise (dTMP/dT, bar/day) with flux; values were 0.03, 0.05, and 0.11 bar/day for tests at 5, 10, and 15 LMH. Additional data for 20 and 35 LMH were obtained from our previous study at the same crossflow velocity, salt, and nutrient conditions, where the dTMP/dT values were 0.21 and 0.62 bar/day at 20 and 35 LMH respectively [12]. The exponential nature of the dTMP/dT versus flux plot suggests

that the rate of membrane fouling may be linked to concentration polarization (see Equation 2). This is discussed further in Section 3.2.

ΔP_{CH} was measured during each experiment. The data are presented as the rate of pressure drop increase ($d\Delta P_{CH}/dT$) (Figure 3a) which increased with flux, with $d\Delta P_{CH}/dT$ values of 0.10, 0.25, and 0.35 kPa/day for fluxes of 5, 10, and 15 LMH, respectively. The degree of dependence of $d\Delta P_{CH}/dT$ on flux was greater than anticipated in our earlier study [12]. If the role of flux at constant crossflow velocity is to increase concentration polarization it should have an impact on membrane fouling, rather than spacer fouling. As described below, the biovolume of biofilm associated with the spacer was relatively independent of flux, so the increased $d\Delta P_{CH}/dT$ cannot be explained by increased spacer biofilm per se. It is suggested that the increased amount of biofilm on the membrane provided a constriction to crossflow resulting in addition pressure drop [16]. In summary from the TMP and ΔP_{CH} data, it was shown that higher flux was associated with faster increase of pressure drop across the membrane between the feed side and the permeate side (TMP), as well as a pressure drop along the membrane feed channel (ΔP_{CH}).

Autopsies of the membranes at the end of the experiments showed that there were differences in biofilm development at the different fluxes (Figures 4 and 5). The spacers comprised of criss-cross filaments (Figure 6). The filaments which are not touching the membrane are defined as “detached filaments”, while the filaments directly touching the membrane surface are defines as “attached filaments”. In Figure 4, a non-uniform coverage of biofilm was evident with less or no coverage on areas under detached spacer filaments where higher shear is expected. For both membrane and spacer biofilms, the amount of live cells (live cells are represented as green in colour, Figure 4) was found to be significantly higher than dead cells (shown in red) for all test conditions. On the membrane surface, the amount of biofilm increased with flux (Figure 5). While on the spacer, non-significant differences in the amount of biofilm were observed. However the biovolume associated with the membrane surface was significantly more than associated with the spacer.

3.1.2. Impact of crossflow velocity

Three different crossflow velocities, 0.10, 0.17, and 0.34 m/s at constant flux (15 LMH), were tested to determine the impact of crossflow velocity on TMP rise (Figure 7). Over a 10 day period, the percent TMP increase was 11% and 9% for 0.10 and

0.17 m/s, respectively (Figure 7a). A dramatic reduction in the percent TMP rise, 4%, was achieved at a crossflow of 0.34 m/s (Figure 7a). The incremental TMP rise from lowest to highest crossflow velocities were 1.0, 0.8 and 0.3 bar (Figure 7b).

Crossflow velocity contributes to the shear force, which decreases CP of solutes, including nutrients. Therefore, higher crossflow velocity should lead to a slower biofouling. Figure 8 shows the dTMP/dT (bar/day) of operations at different crossflow velocities. At 15 LMH, dTMP/dT values were 0.03, 0.09, and 0.10 bar/day for tests at 0.34, 0.17, and 0.10 m/s. Additional data from experiments at 35 LMH are also shown from previous published data for the same crossflow velocity variations [12]; dTMP/dT values from highest to lowest crossflow velocity were 0.13, 0.53, and 0.82 bar/day. It is evident from Figure 8 that higher crossflow velocity resulted in slower biofouling rates and the impact was magnified at higher flux operation.

Autopsies of the membranes showed that the biofilms were not uniformly distributed over the surface of the membrane or the spacers at crossflow velocities of 0.34 and 0.17 m/s (Figure 9). The amount of live cells was also found to be significantly higher for these two crossflow velocities (94% live cells, Figure 10). At the lowest crossflow velocity of 0.10 m/s, biofilm coverage was found to be more uniform (Figure 9) and the percentage of live cells was 68% (Figure 10). Biofilm biovolume on the membrane was significantly higher than on the spacer (Figure 10 and 11). It should be noted that Figure 11 shows the combined live and dead biovolumes. On the membrane surface at 0.10 m/s the total biofilm biovolume was 28.5 $\mu m^3/\mu m^2$, and decreased to 26.3 and 16.5 $\mu m^3/\mu m^2$ at 0.17 and 0.34 m/s respectively. On the feed spacer, biofilm biovolumes from lowest to highest crossflow velocity were 3.5, 6.1, and 5.4 $\mu m^3/\mu m^2$. Thus, it appeared that an increase of crossflow velocity produced reduced amounts of biofilm on the membrane, while on the spacer non-significant differences were observed.

The ΔP_{CH} along the channel was greater at higher crossflow velocity. As shown in Figure 3b, $d\Delta P_{CH}/dT$ increased from 0.09 kPa/day at 0.10 m/s to 0.35 and 0.90 kPa/day at 0.17 and 0.34 m/s, respectively. ΔP_{CH} in the membrane module rises due to channel blockage and obstruction. It has been suggested that biofilm development on the feed spacer is predominantly responsible for ΔP_{CH} rise [17, 18]. The feed channel pressure drop in a membrane channel is given by [19]:

$$\Delta P_{CH} = \frac{\rho u_x^2}{2} \cdot \frac{A'}{\mathrm{Re}^n} \cdot L_{CH}$$ Equation 1

The average cross flow velocity, u_x is increased as the channel voidage, ε, decreases due to build up of foulant on the spacer (the effect on Re^n is minor since n is in the range 0.2 to 0.3, [19]). The channel ΔP_{CH} is very sensitive due to the u_x^2 term. Therefore, an increase in ΔP_{CH} at higher crossflow velocity would be expected (Figure 3b). The sensitivity of ΔP_{CH} to crossflow is discussed further in section 3.3. In our previous work [12] we speculated that $d\Delta P_{CH}/dT$ should be independent of flux. However, Figure 3a shows that this is not correct with an increasing trend of $d\Delta P_{CH}/dT$ with flux. This suggests that the increased fouling on the membrane also contributes to the increase of ΔP_{CH}. The presence of biofilm on the membrane surface may cause channel constriction between the detached filaments and the membrane and decrease the effective cross-sectional area, a scenario which is also experienced in other water systems [20, 21].

3.2. Fouling rate as function of nutrient concentration polarization ($C_{w,N}$)

Our earlier hypothesis was that membrane biofouling is flux-driven with an elevated nutrient level provided by concentration polarization [12]. Therefore to allow comparison among different experimental conditions, the biofouling rate (dTMP/dT) has been plotted versus the estimated polarized nutrient concentration near the membrane surface, $C_{w,N}$ which is a function of crossflow velocity and flux. Based on the Film model for CP calculation, the $C_{w,N}$ may be written as [22]:

$$C_{w,N} = C_{b,N} \exp\left(\frac{J_v}{k_m}\right)$$ Equation 2

where $C_{b,N}$ is the concentration of nutrient in the bulk solution, J_v is the imposed flux and k_m is mass transfer coefficient. The k_m value can be experimentally obtained by using the sodium chloride tracer response technique, where a concentrated sodium chloride solution was injected into the system as a pulse and the response information (TMP, feed and permeate conductivities) were collected for the calculation. This method is described in detail elsewhere [23]. The k_m value at a crossflow velocity 0.17 m/s for the RO spacer-filled channel used in the experiment is approximately 4.4

x 10^{-5} m/s. The k_m at different crossflow velocities may be estimated based on the modified Grober correlation for spacer-filled channels [19],

$$k_m = B\,u_x^{0.5} \qquad \text{Equation 3}$$

where B is a coefficient and u_x is the effective crossflow velocity.

$C_{w,N}$ values were estimated from the experiments at various fluxes and crossflow velocities (Figures 2 and 8). The $C_{w,N}$ (mg/L TOC) values are plotted against the TMP rise rate (dTMP/dT, Bar/day) in Figure 12. It should be noted that since the TMP rise profiles are typically in two stages (a quasi-linear initial stage followed by an accelerated stage) for high fouling rate experiments (35 LMH and 0.17 m/s; 35 LMH and 0.10 m/s) the dTMP/dT values shown in Figure 12 are calculated based on the initial linear section of the total TMP rise to allow fair comparison between low fouling and high fouling experiments.

The plot of $C_{w,N}$ vs dTMP/dT can be extended to include tests without spacer (empty channels). Estimated $C_{w,N}$ values from tests without spacer were obtained from our previous studies at different crossflow velocities [12] and different nutrient levels [24]. Similarly to the calculation for spacer-filled channels, $C_{w,N}$ values were estimated by Equation 2 where the k_m value for the empty channel was also obtained from a salt-pulse tracer experiment (1.4 x 10^{-5} m/s) [25]. The plot of $C_{w,N}$ versus TMP rise rate (dTMP/dT, Bar/day) in the empty channel is shown in Figure 13 together with the plot for spacer-filled channels. The dTMP/dT values were based on the linear section of the TMP rise.

A general trend of faster membrane fouling (higher dTMP/dT) at higher $C_{w,N}$ can be observed from tests with both empty and spacer-filled channels. A slower fouling rate is observed in spacer-filled channels, and this is more significant at low nutrient concentrations, signifying the positive impact of the spacer in reducing fouling. The presence of the spacer causes variability of shear stress and biofilm coverage. Biofilms grown in empty channels showed more uniform membrane coverage than spacer-filled channels [12].

Both plots in Figure 12 and 13 show that there is a reasonable correlation between the concentration of nutrient at the membrane surface and the rate of fouling. This signifies a relationship between the nutrient supply and biofilm growth on the

membrane surface. The trend may be explained by the Monod equation for specific bacterial growth rate (μ_{bio}) when nutrient is limiting [26],

$$\mu_{bio} = \mu_{bio-\max} \frac{C_{w,N}}{K_N + C_{w,N}} \qquad \text{Equation 4}$$

Where $\mu_{bio\text{-}max}$ is the maximum specific growth rate, K_N is the concentration of nutrient at which the rate is half the maximum. When $C_{w,N} << K_N$ the growth rate, μ_{bio}, tends to be linear with $C_{w,N}$.

The spacer data hint at a threshold condition of $C_{w,N}$ where dTMP/dT is very low. This is for the highest shear scenarios where the effect of particulate critical flux could limit the deposition of bacteria on the membrane. However, as discussed below, high crossflow is not a panacea due to the need to control ΔP_{CH} rise.

3.3. Controlling biofouling through hydrodynamic variations

In Section 3.1, the impact of different hydrodynamic conditions on both pressure drops in a membrane module have been demonstrated. Operation at high flux was clearly detrimental to the performance of RO. Increase in pressure drop was suffered both across the membrane (Figure 2) and along the channel (Figure 3a) and additionally, biofilm developed faster on the membrane (Figure 11a).

In full scale desalination plants, multiple pressure vessels are used with each comprised of several membrane elements. It is inevitable that local variation of flux and pressure drop occur. Chen et al. [27] and Hoek et al. [28] have shown in their models that local flux has a downward trend from the lead element to the tail element. They both agree that lead elements suffer more fouling as a consequence of higher imposed flux. However, the effect of recovery will reduce load crossflow and increase nutrient concentration in the tail element. These conditions could also enhance biofilm growth. Results in this study affirms the role of flux in biofouling and suggests that maintaining a moderate local flux over different regions may be able to reduce biofouling and prolong membrane life. Several methods have been proposed to minimize variations among membrane elements including flow reversal [29, 30], membrane elements swapping [31] and the use of hybridization where membranes with different permeability and rejection are used [32].

Crossflow velocity has been shown to reduce biofilm development on the membrane, and subsequently the TMP rise. In Figure 8, the reduction of fouling rate on the membrane is clearly seen. At a flux of 15 LMH the fouling rate was reduced by 70% when the crossflow velocity increased from 0.10 to 0.34 m/s. A more dramatic reduction was achieved at a flux of 35 LMH (85% reduction). Although crossflow velocity was able to reduce TMP rise, an increase of the ΔP_{CH} was encountered (Figure 3b). This is an interesting finding since total biovolume was reduced with crossflow velocity (Figure 11b).

In spacer-filled channels, the effective crossflow velocity, u_x is a function of superficial crossflow velocity, u_v, and channel voidage, ε [19].

$$u_x = \frac{u_v}{\varepsilon} \qquad \text{Equation 5}$$

Therefore, channel pressure drop (ΔP_{CH}) from Eq. 1 may be written as:

$$\Delta P_{CH} = K \cdot \left(\frac{u_v}{1-\varepsilon} \right)^2 \qquad \text{Equation 6}$$

If fouling causes a small change in ε, say $(-\Delta\varepsilon)$. Then:

$$\left(\Delta P_{CH}\right)_{fouled} = K \cdot \left(\frac{u_v}{1-\left(\varepsilon - \Delta\varepsilon\right)} \right)^2 = K \cdot \left(\frac{u_v}{1-\varepsilon+\Delta\varepsilon} \right)^2 \qquad \text{Equation 7}$$

If Δε is assumed similar at different crossflow velocities, Equation 10 predicts more change in $\left(\Delta P_{CH}\right)_{fouled}$ for higher crossflow velocity with $\left(\Delta P_{CH}\right)_{fouled}$ proportional to u_v^2. The ratio of channel pressure drop increase, dP_{CH}/dT and (crossflow velocity)^2 is calculated and summarized in Table 1.

The results in Table 1 can be explained if the Δε due to fouling is not constant but varies with crossflow velocity. This is supported, in part, by Figure 11b where the 0.34 m/s crossflow velocity had the smallest measured biovolumes.

In summary, this study has shown that it is beneficial to consider different hydrodynamic conditions to control biofouling and subsequently to achieve prolonged membrane life and save costs. Maintaining a balanced and modest flux among different membrane elements is important. Similarly, crossflow velocity must be kept

reasonably high to provide good control of CP and subsequent biofouling. One must also note that in a certain condition where nutrient mass transfer is limiting, increase of crossflow velocity may give a higher nutrient loading rate and enhance biofilm growth [33]. It is possible that an optimum crossflow velocity exists that is a trade off between decreasing TMP rise and increasing ΔP_{CH} rise.

4. Conclusions

The experiments presented in this study were designed to simulate RO operations with a steady supply of bacteria and nutrient, fixed permeate production, elevated salinity, and feed channel spacers. However a model bacterium was used to ensure reproducible feed conditions. It was shown that biofouling caused a TMP rise at constant flux and the *ex-situ* observation by CLSM of biofilm formation on the membranes provided details of the developing pattern of the biofouling. Higher flux resulted in faster biofilm build-up on the membrane and increased TMP and ΔP_{CH} rise. The increased ΔP_{CH} was not due to increased biovolume on the spacer but linked to increased biovolume on the membrane, possibly causing flow channel constriction. Raising crossflow velocity reduced biofilm build-up on the membrane and lowered the TMP rise, but increased ΔP_{CH}. For a range of fluxes and crossflows there is a correlation between the estimated nutrient concentrations on the membrane surface due to concentration polarization and the TMP rise due to biofilm growth. The results suggest that RO biofouling may be controlled by limiting incoming nutrient concentration and maintaining modest flux and moderately high crossflow velocity, subject to a trade-off with ΔP_{CH} rise.

Acknowledgements

The authors wish to acknowledge financial support from the Economic Development Board of Singapore and from Nanyang Technological University for the Singapore Membrane Technology Centre and the Advanced Environmental Biotechnology Centre where the work was performed. This project was also partially supported by a grant (MEWR C651/06/177) from the Environment and Water Industry Programme Office of Singapore.

Nomenclature

A'	Constant in eq. 7 (-)
B	Constant used in Grober correlation of mass transfer coefficient and crossflow velocity (m s^{-1})

$C_{b,N}$	concentration of nutrient in the bulk solution (mg L^{-1})
$C_{w,N}$	concentration of nutrient near the membrane surface (mg L^{-1})
J_v	Average flux (L m^{-2} h^{-1} or m^3 m^{-2} s^{-1})
k	Overall mass transfer coefficient (m s^{-1})
k_m	Mass transfer coefficient in the boundary layer (m s^{-1})
K_N	Saturation constant of Nutrient Broth (mg L^{-1})
L_{CH}	Channel length (m)
Re^n	Reynolds number (-)
TMP	Trans-membrane pressure (Pa or bar)
u_v	Volumetric cross flow velocity (m s^{-1})
u_x	Superficial cross flow velocity (m s^{-1})
$dTMP/dT$	Rate of increase of trans-membrane pressure (bar day^{-1})

Greek terms

μ_{bio}	Specific bacterial growth rate (h-1)
$\mu_{bio-\max}$	Maximum specific bacterial growth rate (h-1)
ΔP_{CH}	Channel pressure drop (Pa or bar)
ε	Voidage (-)
ρ	Density of solution (kg m^{-3})
$d\Delta P_{CH}/dT$	Rate of increase of channel pressure drop (kPa day^{-1})

References

[1] P. Watnick, R. Kolter, Biofilm, city of microbes, Journal of Bacteriology, 182 (2000) 2675-2679.

[2] H.C. Flemming, Reverse osmosis membrane biofouling, Experimental Thermal and Fluid Science, 14 (1997) 382-391.

[3] T.H. Chong, F.S. Wong, A.G. Fane, The effect of imposed flux on biofouling in reverse osmosis: Role of concentration polarisation and biofilm enhanced osmotic pressure phenomena, Journal of Membrane Science, 325 (2008) 840-850.

[4] M. Herzberg, M. Elimelech, Biofouling of reverse osmosis membranes: Role of biofilm-enhanced osmotic pressure, Journal of Membrane Science, 295 (2007) 11-20.

[5] A. Subramani, E.M.V. Hoek, Direct observation of initial microbial deposition onto reverse osmosis and nanofiltration membranes, Journal of Membrane Science, 319 (2008) 111-125.

[6] H.A. Munshi, M.O. Saeed, T.N. Green, A.A. Al-Hamza, F.M. A., A.R.A. Ismail, Impact of UV Irradiation on Controlling Biofouling Problems in NF-SWRO Desalination Process, in: International Desalination Association (IDA) World Congress, Singapore, 2005.

[7] T. Nguyen, F.A. Roddick, L. Fan, Biofouling of water treatment membranes: A review of the underlying causes, monitoring techniques and control measures, Membranes, 2 (2012) 804-840.

[8] F.A. Abd El Aleem, K.A. Al-Sugair, M.I. Alahmad, Biofouling problems in membrane processes for water desalination and reuse in Saudi Arabia, International Biodeterioration and Biodegradation, 41 (1998) 19-23.

[9] J. Gutman, S. Fox, J. Gilron, Interactions between biofilms and NF/RO flux and their implications for control-A review of recent developments, Journal of Membrane Science, 421-422 (2012) 1-7.

[10] M. Herzberg, S. Kang, M. Elimelech, Role of extracellular polymeric substances (EPS) in biofouling of reverse osmosis membranes, Environmental Science and Technology, 43 (2009) 4393-4398.

[11] M. Herzberg, M. Elimelech, Physiology and genetic traits of reverse osmosis membrane biofilms: A case study with Pseudomonas aeruginosa, ISME Journal, 2 (2008) 180-194.

[12] S.R. Suwarno, X. Chen, T.H. Chong, V.L. Puspitasari, D. McDougald, Y. Cohen, S.A. Rice, A.G. Fane, The impact of flux and spacers on biofilm development on reverse osmosis membranes, Journal of Membrane Science, 405-406 (2012) 219-232.

[13] L.F. Greenlee, D.F. Lawler, B.D. Freeman, B. Marrot, P. Moulin, Reverse osmosis desalination: Water sources, technology, and today's challenges, Water Research, 43 (2009) 2317-2348.

[14] J. Daugherty, S. Deshmukh, M. Patel, K. Alexander, D. Cutler, Applying advanced membrane technology for Orange County's water reuse treatment facilities, in: K.J. Howe (Ed.) Membrane Treatment for Drinking Water & Reuse Applications: A Compendium of Peer-Reviewed Papers, American Water Works Association, Denver, 2006, pp. 539-564.

[15] M.O. Saeed, A.T. Jamaluddin, I.A. Tisan, D.A. Lawrence, M.M. Al-Amri, K. Chida, Biofouling in a seawater reverse osmosis plant on the Red Sea coast, Saudi Arabia, Desalination, 128 (2000) 177-190.

[16] Woods Hole Oceanographic Institute, The Effects of Fouling, in: Marine Fouling and Its Prevention, U.S. Naval Institute, Anapolis, Maryland, 1952.

[17] J.S. Vrouwenvelder, D.A. Graf von der Schulenburg, J.C. Kruithof, M.L. Johns, M.C.M. van Loosdrecht, Biofouling of spiral-wound nanofiltration and reverse osmosis membranes: A feed spacer problem, Water Research, 43 (2009) 583-594.

[18] J.S. Vrouwenvelder, J.A.M. van Paassen, J.M.C. van Agtmaal, M.C.M. van Loosdrecht, J.C. Kruithof, A critical flux to avoid biofouling of spiral wound nanofiltration and reverse osmosis membranes: Fact or fiction?, Journal of Membrane Science, 326 (2009) 36-44.

[19] A.R. Da Costa, A.G. Fane, D.E. Wiley, Spacer characterization and pressure drop modelling in spacer-filled channels for ultrafiltration, Journal of Membrane Science, 87 (1994) 79-98.

[20] T.R. Bott, Techniques for reducing the amount of biocide necessary to counteract the effects of biofilm growth in cooling water systems, Applied Thermal Engineering, 18 (1998) 1059-1066.

[21] K.V.K. Nair, Marine biofouling and its control with particular reference to condenser-cooling circuits of power plants - an overview, Journal of the Indian Institute of Science, 79 (1999) 497-511.

[22] M. Mulder, Basic principles of membrane technology, Kluver Academic Publishers, Dordrecht, 1991.

[23] T.H. Chong, F.S. Wong, A.G. Fane, Enhanced concentration polarization by unstirred fouling layers in reverse osmosis: Detection by sodium chloride tracer response technique, Journal of Membrane Science, 287 (2007) 198-210.

[24] X. Chen, S.R. Suwarno, T.H. Chong, D. McDougald, S. Kjelleberg, Y. Cohen, A.G. Fane, S.A. Rice, Dynamics of biofilm formation under different nutrient levels and the effect on biofouling of a reverse osmosis membrane system, Biofouling, 29 (2013) 319-330.

[25] S.R. Suwarno, Biofouling in Reverse Osmosis Water Reclamation and Desalination, Ph.D. Thesis, Nanyang Technological University, Singapore, 2013.

[26] J. Monod, The Growth of Bacterial Cultures, Annual Review of Microbiology, 3 (1949) 371-394.

[27] K.L. Chen, L. Song, S.L. Ong, W.J. Ng, The development of membrane fouling in full-scale RO processes, Journal of Membrane Science, 232 (2004) 63-72.

[28] E.M.V. Hoek, J. Allred, T. Knoell, B.H. Jeong, Modeling the effects of fouling on full-scale reverse osmosis processes, Journal of Membrane Science, 314 (2008) 33-49.

[29] J. Gilron, M. Waisman, N. Daltrophe, N. Pomerantz, M. Milman, I. Ladizhansky, E. Korin, Prevention of precipitation fouling in NF/RO by reverse flow operation, Desalination, 199 (2006) 29-30.

[30] N. Pomerantz, Y. Ladizhansky, E. Korin, M. Waisman, N. Daltrophe, J. Gilron, Prevention of scaling of reverse osmosis membranes by "zeroing" the elapsed nucleation time. Part I. Calcium sulfate, Industrial and Engineering Chemistry Research, 45 (2006) 2008-2016.

[31] S.S. Madaeni, M. Afshar, N. Jaafarzadeh, F. Tarkian, K. Ghasemipanah, Rearrangement of membrane elements in the pressure vessels for optimum utilization of reverse osmosis process, Chemical Engineering Research and Design, 89 (2011) 48-54.

[32] R.N. Franks, C.R. Bartels, V.S. Frenkel, D. Birch, Evaluating the economics of a unique hybrid RO design after three years of treating brackish groundwater, Hydranautics/Nitto Denko, (2012).

[33] J.S. Vrouwenvelder, C. Hinrichs, W.G. Van der Meer, M.C. Van Loosdrecht, J.C. Kruithof, Pressure drop increase by biofilm accumulation in spiral wound RO and NF membrane systems: role of substrate concentration, flow velocity, substrate load and flow direction, Biofouling, 25 (2009) 543-555.

Figures and table

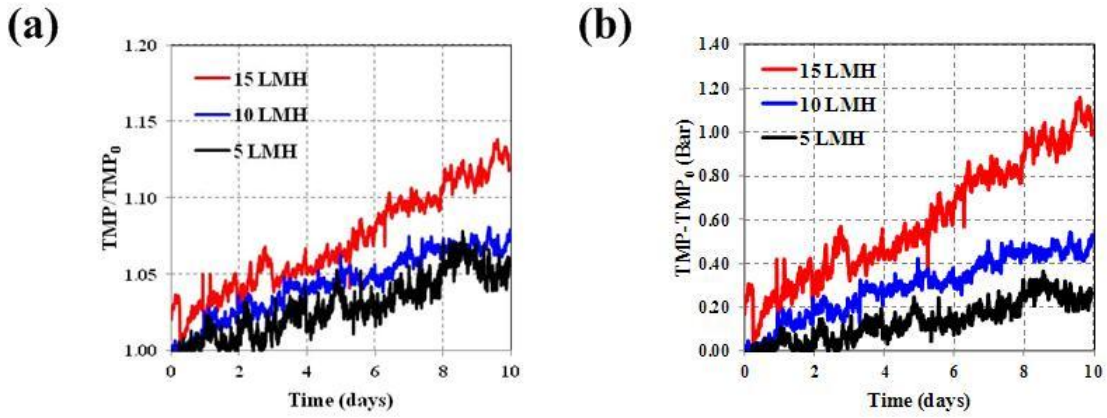

Figure 1. Profiles of (a) normalized TMP rise and (b) relative TMP rise of the RO system at different fluxes of 5, 10, and 15 LMH. NaCl concentration = 4,000 mg/L, nutrient broth = 20 mg/L, crossflow velocity = 0.17 m/s.

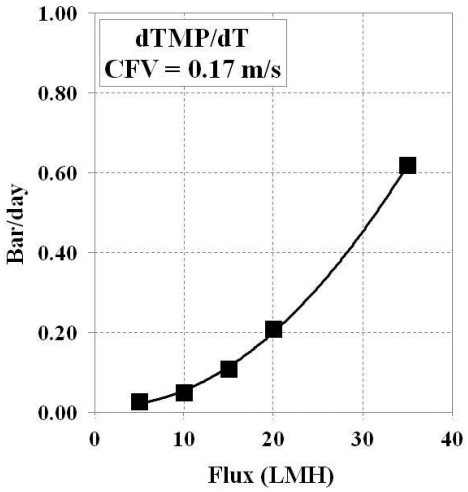

Figure 2. Rate of TMP rise (dTMP/dT) of the RO system at different fluxes of 5, 10, 15, 20, and 35 LMH. The data for 20 and 35 LMH were taken from our previous study [12].

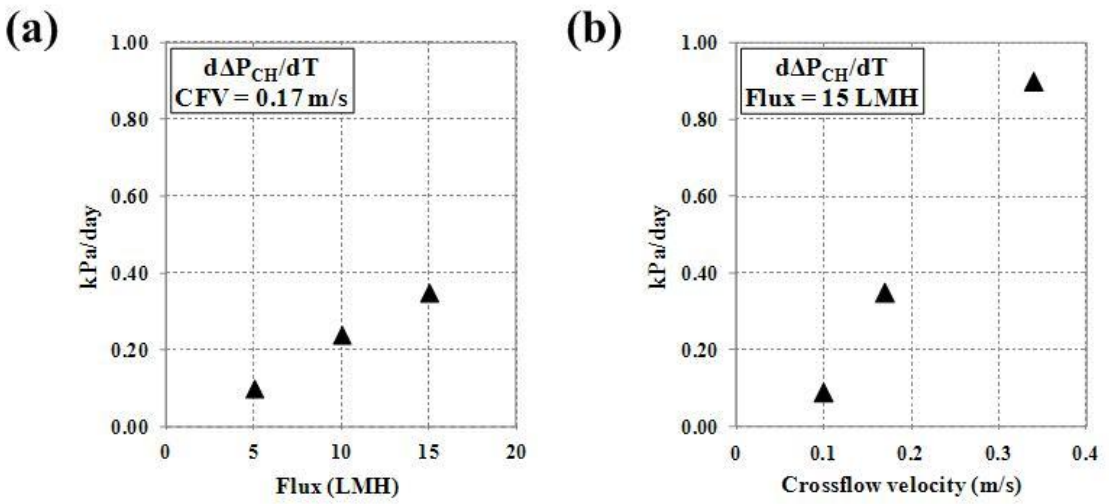

Figure 3. Rate of ΔP_{CH} increase ($d\Delta P_{CH}/dT$) of the RO system at (a) crossflow velocity of 0.17 m/s and different fluxes of 5, 10, and 15 LMH, and (b) flux of 15 LMH and different crossflow velocities of 0.10, 0.17, and 0.34 m/s.

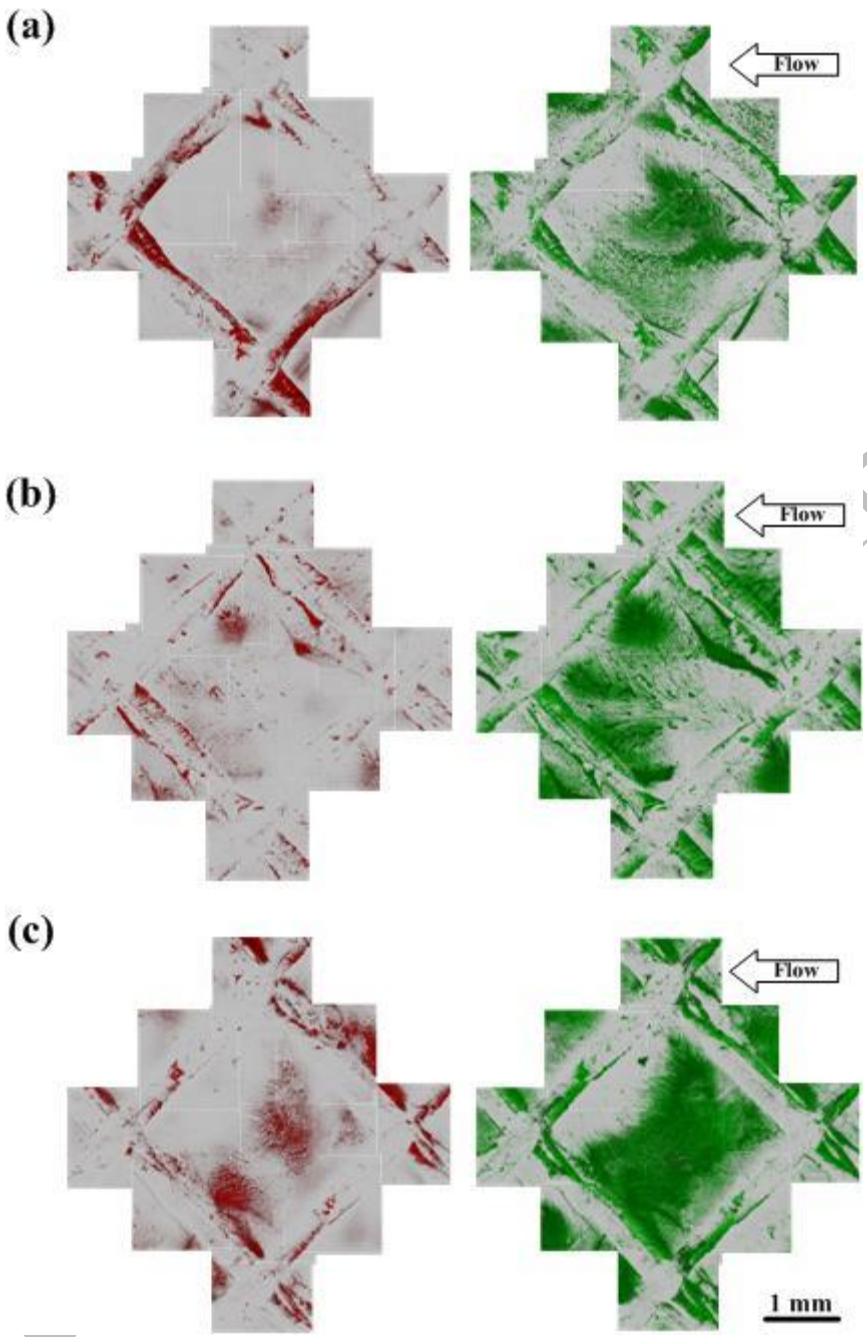

Figure 4. Confocal microscopic images of the biofilms on the RO membranes and spacers under different fluxes: (a) 5 LMH, (b) 10 LMH, and (c) 15 LMH. *P. aeruginosa* PAO1 was inoculated into the RO system and allowed to form biofilms. At the time point of 10 d, membranes and spacers were removed for autopsy and fluorescently stained with Live/Dead stains, in which the live cells are green and the dead are red.

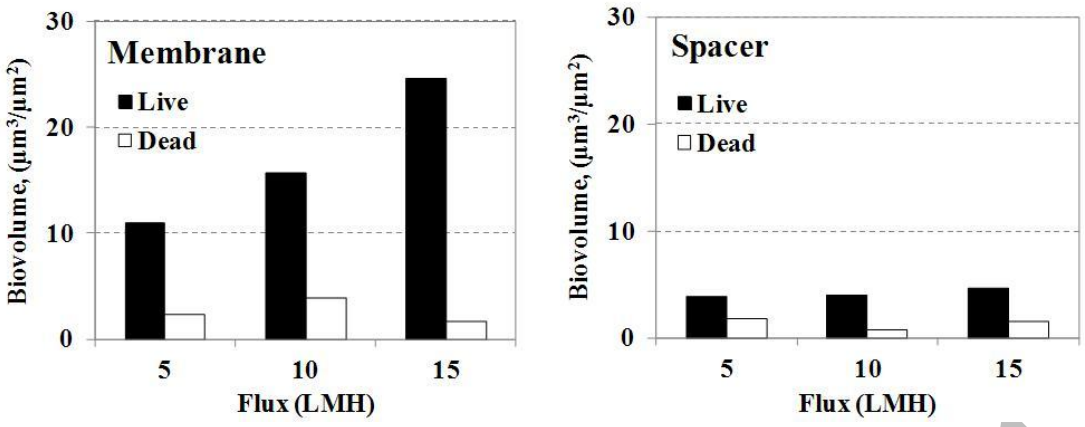

Figure 5. The biovolume ($\mu m^3/\mu m^2$) of live and dead cells calculated using IMARIS on the RO membranes and spacers under different fluxes of 5, 10, and 15 LMH. *P. aeruginosa* PAO1 was inoculated into the RO system and allowed to form biofilms. Membranes and spacers were removed for autopsy on day 10.

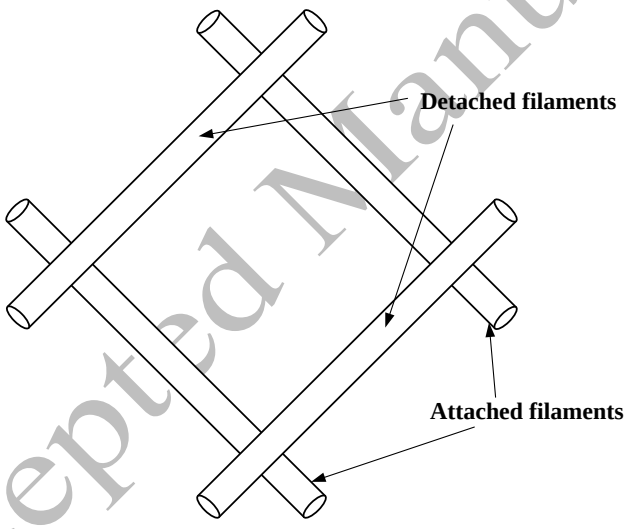

Figure 6. Diagram of spacer filaments not touching the membrane (detached filaments) and touching the membrane (attached filaments).

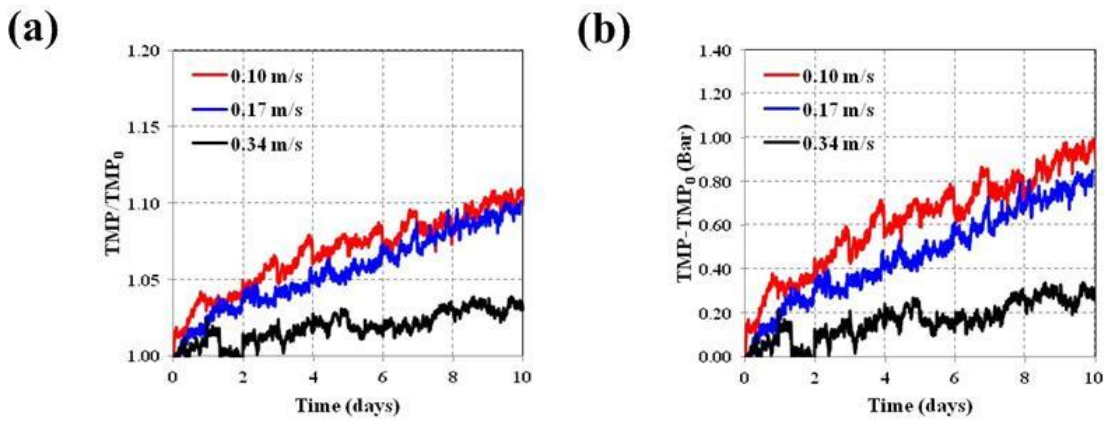

Figure 7. Profiles of (a) normalized TMP rise and (b) relative TMP rise of the RO system at different crossflow velocities of 0.10, 0.17, and 0.34 m/s. NaCl concentration = 4,000 mg/L, nutrient broth = 20 mg/L, Flux = 15 LMH.

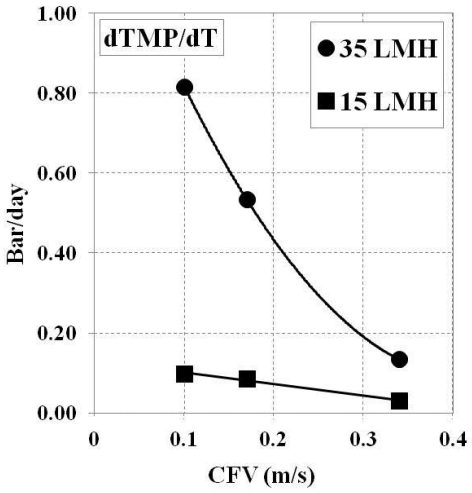

Figure 8. Rate of TMP rise (dTMP/dT) at different crossflow velocities of 0.10, 0.17, and 0.34 m/s. The data for 35 LMH are from our previous study [12].

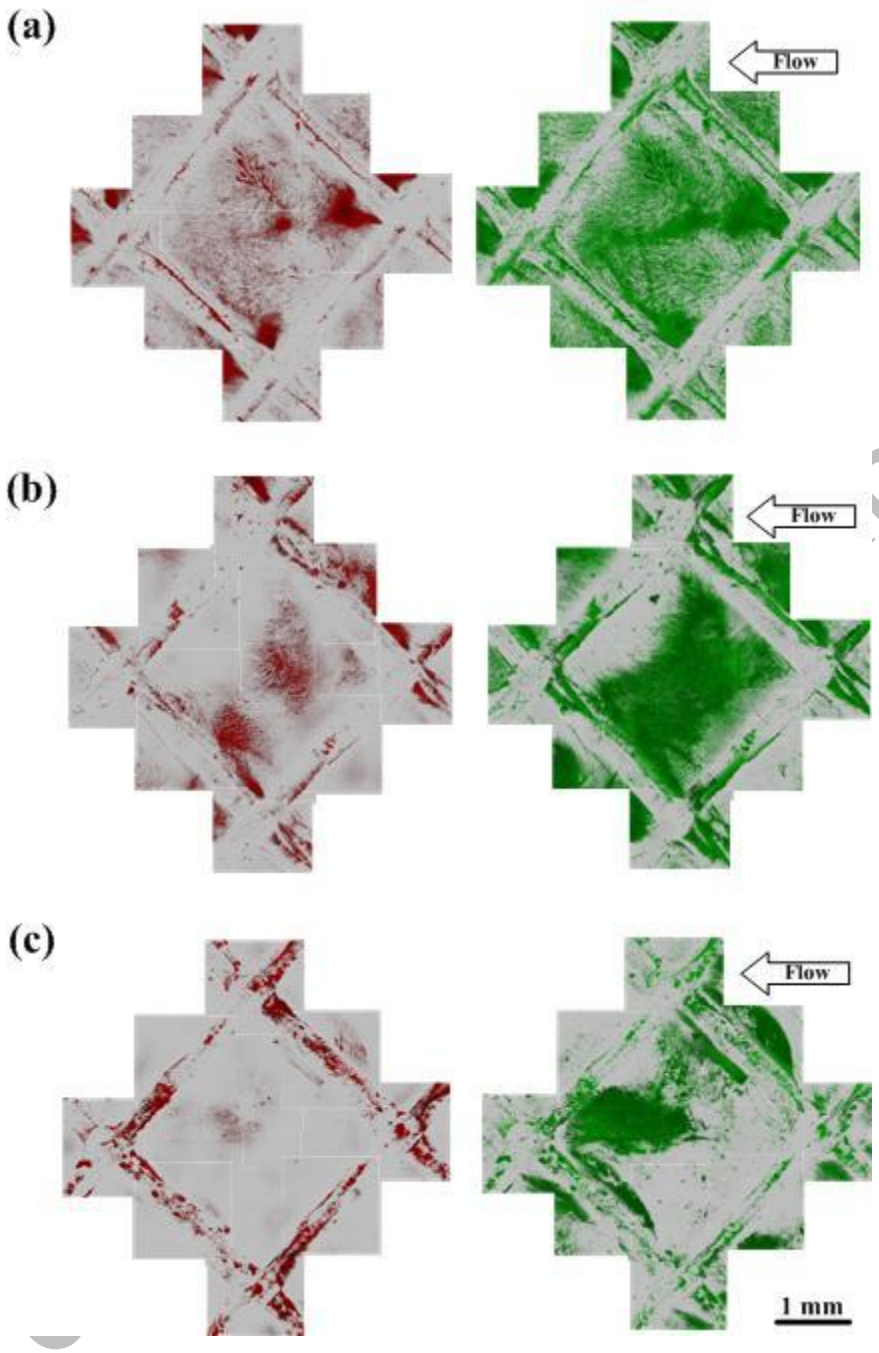

Figure 9. Confocal microscopic images of the biofilms on the RO membranes and spacers under different crossflow velocities: (a) 0.10 m/s, (b) 0.17 m/s, and (c) 0.34 m/s. *P. aeruginosa* PAO1 was inoculated into the RO system and allowed to form biofilms. At the time point of 10 d, membranes and spacers were removed for autopsy and fluorescently stained with Live/Dead stains, in which the live cells are green and the dead are red.

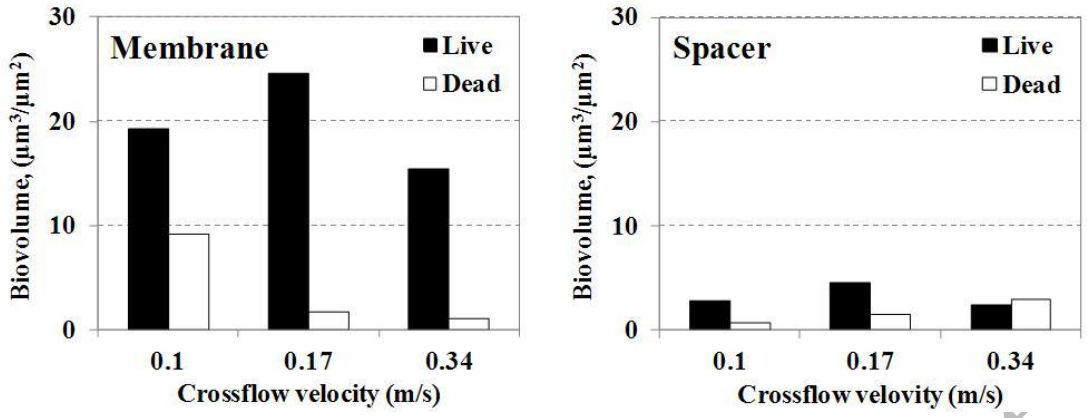

Figure 10. The biovolume ($\mu m^3/\mu m^2$) of live and dead cells calculated using IMARIS on the RO membranes and spacers under different crossflow velocities of 0.10, 0.17, and 0.34 m/s. *P. aeruginosa* PAO1 was inoculated into the RO system and allowed to form biofilms. Membranes and spacers were removed for autopsy on day 10.

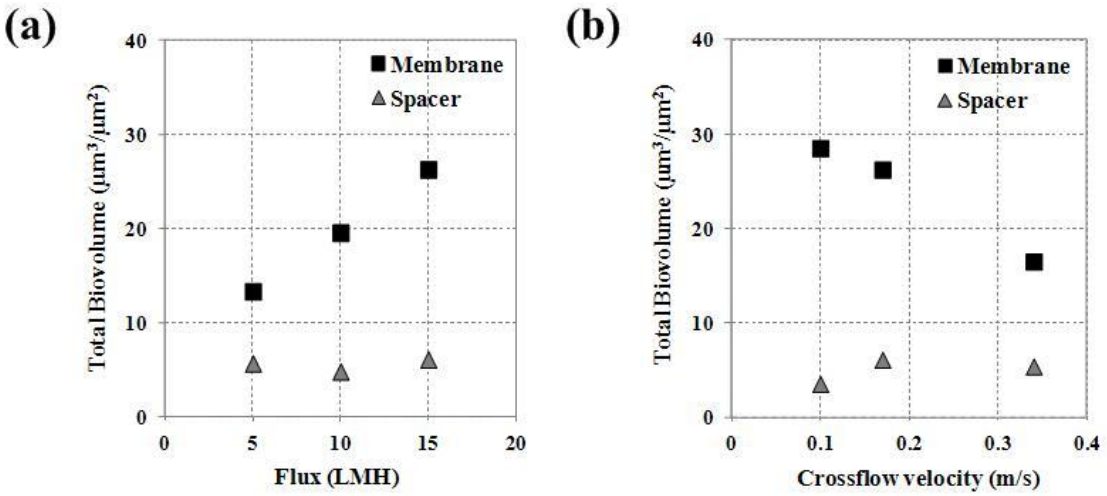

Figure 11. Relative distribution of total biofilm biovolume on the RO membranes and spacers at (a) different fluxes of 5, 10, and 15 LMH and (b) different crossflow velocities of 0.10, 0.17, and 0.34 m/s.

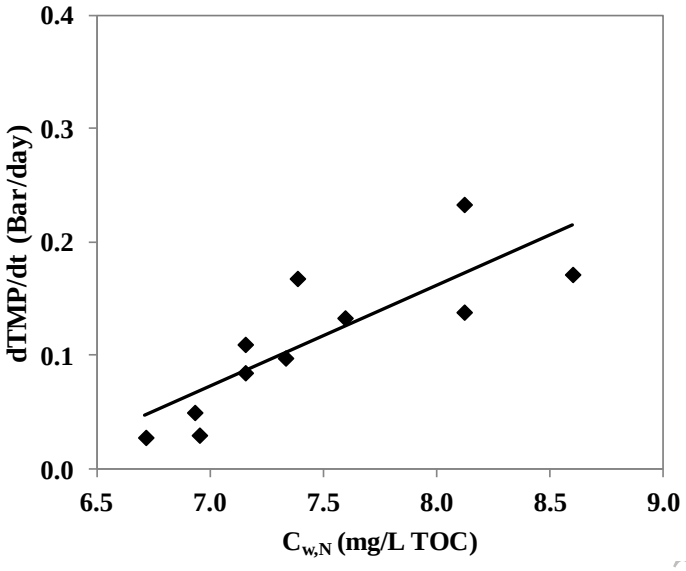

Figure 12. $C_{w,N}$ versus TMP rise rate in spacer-filled channels based on linear section of TMP rise.

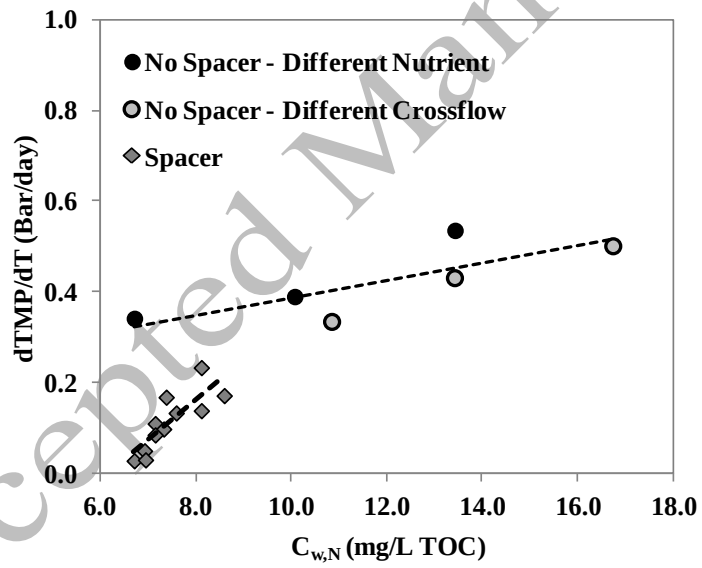

Figure 13. $C_{w,N}$ versus TMP rise rate in empty channels (black and grey circles) and spacer-filled channels (grey diamonds) based on linear section of TMP rise.

Table 1. Ratio of channel pressure drop increase (dP_{CH}/dT) to the superficial crossflow velocity (u_v)

Crossflow velocity (u_v) (m/s)	dP_{CH}/dT (kPa/day)	$\frac{dP_{CH}/dT}{(u_v)^2}$
0.10	0.09	9.0
0.17	0.35	12.1
0.34	0.90	7.8